

Supporting Information for:

**Damping of the Acoustic Vibrations of a Suspended Gold Nanowire in Air and
Water Environments**

Todd A. Major,^a Aurélien Crut,^b Bo Gao,^c Shun Shang Lo,^a Natalia Del Fatti,^b Fabrice
Vallée,^b and Gregory V. Hartland^{a,*}

^a *Department of Chemistry and Biochemistry, University of Notre Dame, Notre Dame, IN
46556, USA*

^b *Université Lyon 1, CNRS, LASIM, 43 Boulevard du 11 Novembre, 69622 Villeurbanne
cedex, France*

^c *Radiation Laboratory, University of Notre Dame, Notre Dame, IN 46556, USA*

* Corresponding author: e-mail ghartlan@nd.edu

Finite Element Calculations:

The acoustic modes of the nanowires were calculated using the Finite Element method implemented through the Solid Mechanics module of Comsol Multiphysics (Version 4.2). The accuracy and speed of these calculations depends on the mesh size, and for the long nanowires in the present study there is a considerable advantage to performing the calculations in two dimensions. This strictly corresponds to an infinitely long nanowire, which is consistent with the analytical results of Equations (1) and (2) of the main text. The 2D analysis only provides information about vibrational modes that are symmetric along the axis of the nanowire. However, this is not a problem for the present studies, as these are the modes that are excited in the transient absorption experiments. Note that we have previously shown that the frequency of the breathing mode of a finite circular cylinder is essentially the same as that for an infinite cylinder for aspect ratios greater than 3,¹ which justifies the approach used here.

The calculations were performed using free boundary conditions with elastic constants of bulk polycrystalline gold, specifically, values of Young's modulus, Poisson's ratio and density of $E = 79$ GPa, $\nu = 0.42$ and $\rho = 19,300$ kg/m³, respectively.² The results from this analysis are presented in scaled frequency units: f/f_c where f_c is the frequency of the breathing mode of a circular cylinder. In these calculations the frequencies were also scaled by the square root of the cross-sectional area, to account for changes in size as the geometry is changed. Different shapes were considered corresponding to NWs with equilateral triangular, square, pentagonal, hexagonal and circular cross-sections.

We first examine the acoustic modes of a circular cylinder. Figure S1(A) shows the mode shapes for the fundamental, and first and second overtones of the breathing mode. The frequencies of these modes agree excellently with the analytical calculations (Equations (1) and (2) of the main text). For example, for a 50 nm radius cylinder we calculate frequencies for the fundamental and 1st and 2nd overtones of 23, 56 and 89 GHz, respectively. In addition to the breathing modes, there are a number of other acoustic modes. Importantly, there are a series of surface modes that resemble “whispering gallery” modes. Each of these modes is doubly degenerate in our 2D model, and the modes with 4-, 5- and 6-fold symmetry are shown in Figure S1(B), along with a high-order surface mode with 22-fold symmetry.

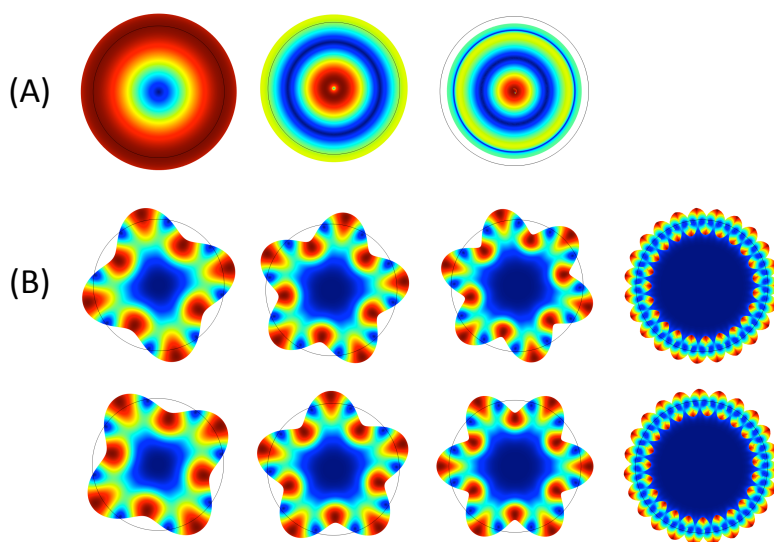


Figure S1: (A) Deformation plots of the mode shapes for the fundamental, 1st overtone and 2nd overtone of the breathing mode of a circular cylinder, calculated with the 2D Finite Element method. (B) Mode shapes (from left-to-right) for surface modes with 4-, 5- and 6-fold symmetry. Also shown is a higher order surface mode with 22-fold symmetry in this series.

Figure S2 shows a plot of the frequencies of the whispering-gallery like acoustic modes versus mode symmetry (the number of lobes in the deformation plots). The frequencies have been normalized to the frequency of the fundamental breathing mode. Note that the 5- and 6-fold symmetry modes are close in frequency to the fundamental breathing mode. The line is a phenomenological fit to the frequencies of the whispering-gallery like modes of $f/f_c = 0.17(n+1)$, where n is the mode symmetry.

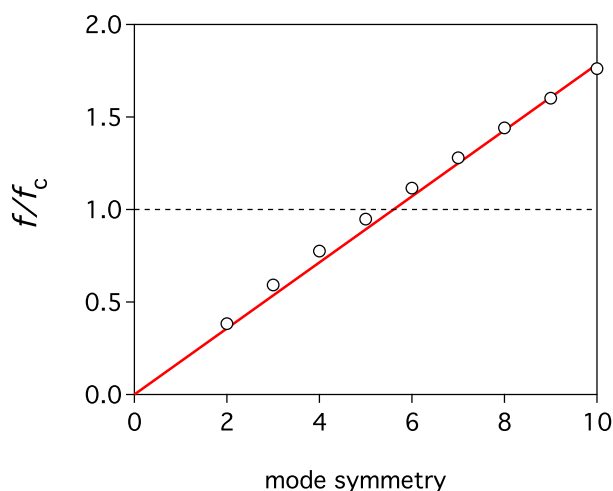


Figure S2: Normalized frequency f/f_c versus mode symmetry for the “whispering-gallery” acoustic modes.

The excitation amplitude of the different modes in the transient absorption experiments was determined by projecting the initial displacement (assumed to be isotropic expansion) onto the orthogonal basis of vibrational modes.^{3,4} For our 2D model, this is done in Comsol by evaluating for each mode its scalar product with the dilation field by computing the surface integral $\iint (u.x + v.y) dS$, where (x,y) and (u,v) are the displacement fields associated to the initial dilation and to the considered normal mode. The scalar product was normalized by dividing by the norms associated to the two fields

$\sqrt{\iint (x^2 + y^2) dS}$ and $\sqrt{\iint (u^2 + v^2) dS}$ to give the excitation amplitude in the transient absorption experiments⁴ (note that the additional effect of the optical detection of vibrational modes in the time-resolved experiments was not included in these calculations). The results of this calculation are presented in Figure S3 (A) for the different shapes considered.

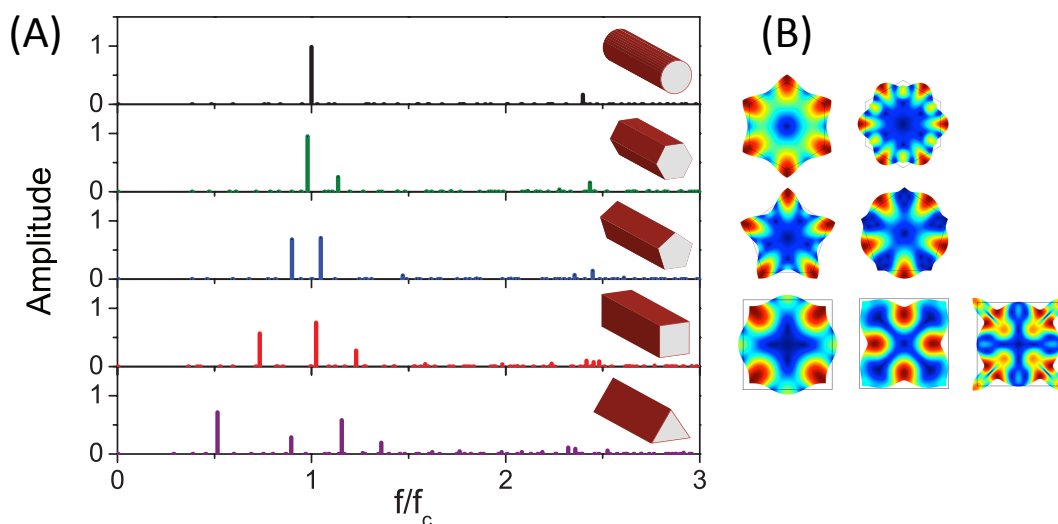


Figure S3: (A) Excitation amplitudes of vibrational modes versus their normalized frequency for different shaped nanowires, in the context of a pump-probe experiment. (B) Deformation plot of the mode shapes for the main modes observed in the spectrum for nanowires with (from top-to-bottom) hexagonal, pentagonal and square cross-sections. The modes are ordered in increasing frequency from left-to-right.

For an infinite circular cylinder, the calculations predict that the vibrational response will be dominated by the fundamental breathing mode, with a small contribution from the 1st overtone. The whispering-gallery like modes discussed above make no contribution to the transient absorption signal: their excitation amplitude is zero. The

situation is different for the other shapes considered – multiple acoustic modes appear, with the spectrum becoming more complicated as the symmetry is reduced. The mode shapes of the main modes that appear in the spectrum are given in Figure S3 (B) for infinite cylinders with hexagonal, pentagonal and square cross-sections. The modes are presented from left-to-right in order of increasing frequency.

The modes that appear in the spectrum are clearly hybrid modes that arise from mixing between the breathing mode and the whispering-gallery like modes that have the symmetry of the nanowire. The lower frequency mode primarily involves motion at the apexes and the higher frequency mode involves motion on the faces on the structure. For the square cross-section there is an additional higher frequency mode in the spectrum that arises from hybridization between the breathing mode and a more complicated 4-fold symmetric acoustic mode. It is important to note that the positions of the modes that appear in the spectrum are determined by the frequencies of the whispering-gallery like modes that mix with the breathing mode. For example, there is a wider spacing between modes for the triangular cross-section nanowire, because the 3-fold symmetric whispering-gallery like mode is much lower frequency than the breathing mode.

Having established the origin of the modes in the transient absorption spectrum, we now examine the effect of rounding the apexes of the pentagonal structure on the frequencies and weights of the acoustic modes. This effect was investigated because real nanowires do not have perfect pentagonal cross-sections: there is some degree of rounding of the apexes.⁵ Rounded apexes were created using the “Fillet” command in Comsol. This is equivalent to placing a circle with radius r at the apex so that it just touches the edges of the structure, and tracing the line created by the circle and the edges

of the structure. For a pentagon, the center of the circle is displaced from the apex by a distance $d = r/\sin(\varphi/2)$ where $\varphi = 108^\circ$ is the angle of the apex. As the radius-of-curvature increases the shape approaches a circle. The limiting radius-of-curvature occurs when the $d = R$, where R is the distance from the center of the pentagon to the apex. This defines a critical radius-of-curvature $r_c = R\sin(\varphi/2)$.

Figure 3 of the main text shows the frequencies and weights of the two main modes versus the relative radius-of-curvature r/r_c for a pentagonal nanowire. The frequencies in Figure 3 are presented as f/f_c where f_c is the frequency for the circular cylinder with a radius r_c . The frequencies have also been scaled by the square-root of the area A of the structure ($\sqrt{A/\pi r_c^2}$), to account for the slight change in size of the object as the radius-of-curvature at the apexes changes. The weights of the modes in the transient absorption experiments were calculated using the formalism given above. Mode shapes are also presented for different values of r/r_c .

Experimental Data:

Additional transient absorption traces for suspended Au nanowires are presented in Figure S4. Examples are given for a NW that displays a single frequency (top) as well as a NW with a double frequency (bottom). The insets of the Figures show Fourier Transforms of the modulated portion of the transient absorption data for the nanowires in air. Scattered light and AFM images of the NW with the double frequency are also presented, which show that this object is an isolated, single NW. Traces are presented for both air and water environments.

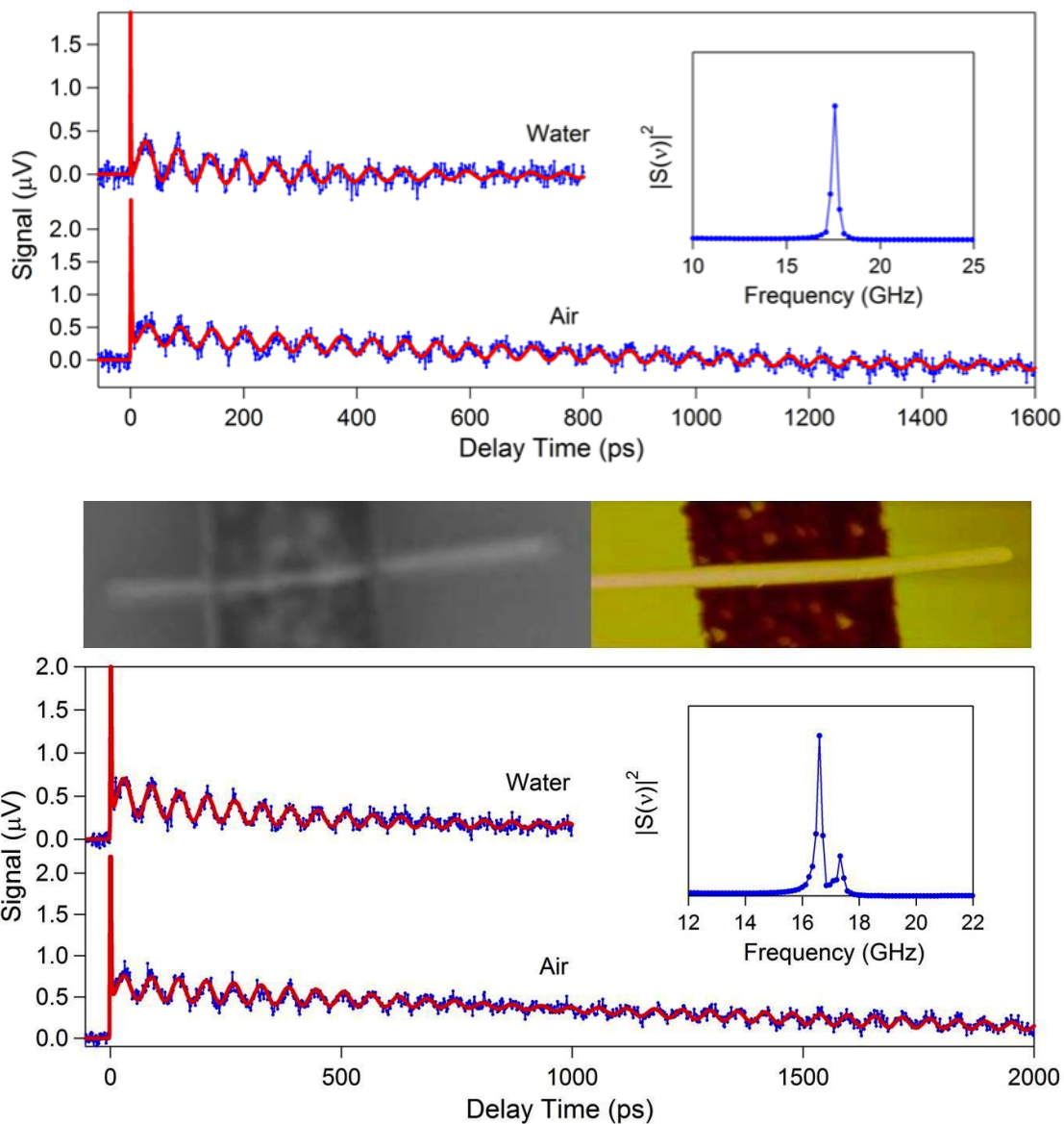


Figure S4: Transient absorption traces for single suspended Au NWs in air and water. Top: NW that displays a single frequency. Bottom: NW with a double frequency. Also shown are scattered light (left) and AFM (right) images of the NW with the double frequency.

Tables S1 and S2 contain the periods and lifetimes extracted from the experimental transient absorption traces for the all the nanowires examined in this paper,

see main text for details. Fits to the transient absorption data were performed using Igor Pro (Version 6.02a).

Table S1: Periods (T_{br}) and lifetimes (τ_{br}) for nanowires with a single vibrational period in air, on glass, and in water.

Wire #	Diameter (nm)	Air		Glass		Water	
		T_{br} (ps)	τ_{br} (ps)	T_{br} (ps)	τ_{br} (ps)	T_{br} (ps)	τ_{br} (ps)
1	135 ± 5	52.8 ± 0.8	1380 ± 80	54.6 ± 0.2	520 ± 80	***	***
2		50.8 ± 0.3	1830 ± 120	52.0 ± 0.2	630 ± 70	***	***
3		55.7 ± 0.3	730 ± 80	55.6 ± 0.2	770 ± 50	***	***
4		53.5 ± 0.3	2200 ± 300	56.5 ± 0.2	370 ± 30	***	***
5	104 ± 5	42.0 ± 0.1	1460 ± 80	41.4 ± 0.1	500 ± 20	42.0 ± 0.1	340 ± 20
6		55.1 ± 0.1	1660 ± 30	57.0 ± 0.1	340 ± 30	55.5 ± 0.1	610 ± 20
7		56.7 ± 0.3	1700 ± 200	60.8 ± 0.1	430 ± 30	57.4 ± 0.5	450 ± 30
8		56.6 ± 0.1	1010 ± 50	58.2 ± 0.1	400 ± 30	56.7 ± 0.1	390 ± 30

Table S2: Periods (T_{br}) and lifetimes (τ_{br}) for suspended nanowires with two vibrational periods in air and in water.

Wire #	Diameter (nm)	Air		Water	
		T_{br} (ps)	τ_{br} (ps)	T_{br} (ps)	τ_{br} (ps)
9	159 ± 5	63.1 ± 0.3 66.9 ± 0.3	2900 ± 500 1900 ± 200	65.8 ± 0.2	240 ± 20
10	145 ± 5	58.0 ± 0.1 60.3 ± 0.1	1900 ± 400 2000 ± 200	60.0 ± 0.1	500 ± 40
11		54.6 ± 0.2 57.1 ± 0.2	2000 ± 500 1400 ± 200		
12		63.2 ± 0.2 66.0 ± 0.2	1700 ± 300 1100 ± 200	64.8 ± 0.2	440 ± 40
13		62.1 ± 0.8 65.1 ± 0.8	1700 ± 400 5000 ± 2000	64.5 ± 0.2	360 ± 30

Absorption Cross-Section Calculations and Laser Induced Heating:

Low powers were used in these experiments to avoid damaging the nanowires. This is especially important in this study, because the same wire must be interrogated in different environments to extract the effect of the environment on vibrational damping.

In this section we estimate the temperature rise in the material induced by the pump and probe lasers. This is done by first calculating the power ΔP absorbed by the nanowire⁶

$$\frac{\Delta P}{P} = \left(\frac{\sigma_{\text{NW}}}{w_0} \right) \sqrt{\frac{2}{\pi}} \quad (\text{S1})$$

where σ_{NW} (units of m for a one-dimensional nano-object) is the absorption cross-section of the nanowire, w_0 is the spot size of the laser, which is assumed to be a Gaussian beam.⁷ Circularly polarized light is used in our experiments, which means that $\sigma_{\text{NW}} = (\sigma_{\text{TM}} + \sigma_{\text{TE}})/2$, where σ_{TM} and σ_{TE} are the cross-sections for transverse magnetic and transverse electric laser polarizations, respectively. The spot size of the laser beams was determined to be $w_0 \approx \lambda/2$ for our experimental system.

Values of σ_{NW} were calculated through the Electromagnetic Waves module of Comsol Multiphysics (Version 4.2). The simulations were again done in 2D, modeling the nanowires as a circular cylinder with perfectly matched layers for the far-field boundaries, and solving for the scattered field. The absorption coefficients were calculated by integrating the adsorbed power (Qrh in Comsol) over the domain of the NW, and dividing by the incident flux ($n_{\text{med}} * P_0$). Calculations were performed for the pump ($\lambda = 720$ nm) and probe ($\lambda = 530$ nm) beams in air ($n_{\text{med}} = 1$) and water ($n_{\text{med}} = 1.33$) environments, using the dielectric constants for bulk gold.⁸ The values obtained for a 50 nm radius nanowire in water are $\sigma_{\text{NW}} = 6.8 \times 10^{-8}$ m at 530 nm and 4.5×10^{-9} m at 720 nm, and for air the cross-sections are $\sigma_{\text{NW}} = 4.8 \times 10^{-8}$ m at 530 nm and 4.0×10^{-9} m at 720 nm.

The temperature rise was then calculated from the heat capacity of the NW and the adsorbed energy per pulse: $\Delta T = \Delta P / (mC \times R)$, where ΔP was calculated from

Equation (S1), R is the repetition rate of the laser (80 MHz), C is the specific heat of Au ($0.129 \text{ J g}^{-1} \text{ K}^{-1}$) and m is the mass of the irradiated portion of the nanowire. The mass is given by $m = (\pi r^2 \sqrt{2} w_0) \rho$, where ρ is the density of gold ($19.3 \times 10^6 \text{ g/m}^3$), r is the radius of the nanowire and $\sqrt{2} w_0$ is the diameter of the equivalent top hat beam. Using energies per pulse of $P/R = 5 \text{ pJ}$ for the pump beam 0.1 pJ for the probe beam, we calculate a temperature rise in the NW of less than 10 K (5K from the pump beam and 2 K from the probe beam) for $r = 50 \text{ nm}$. The energies per pulse at the sample were estimated by measuring the power of the laser just before the microscope, and after the pump and probe had been re-collimated by the second objective, in order to account for optical losses through the focusing objective. The calculated temperature rises are very small, and indicate that the NWs should not be damaged during our experiments.

References:

- 1 A. Crut, P. Maioli, N. Del Fatti and F. Vallée, *Phys. Chem. Chem. Phys.*, 2009, **11**, 5882-5888.
- 2 G. Simmons and H. Wang, *Single Crystal Elastic Constant and Calculated Aggregate Properties: A Handbook*, 2nd Ed. The M.I.T. Press: 1971
- 3 M. Hu, X. Wang, G. V. Hartland, P. Mulvaney, J. P. Juste and J. E. Sader, *J. Am. Chem. Soc.* 2003, **125**, 14925-14933.
- 4 A. Crut, V. Juvé, D. Mongin, P. Maioli, N. Del Fatti and F. Vallée, *Phys. Rev. B*, 2011, **83**, 205430.
- 5 K. Critchley, K. P. Khanal, M. L. Gorzny, L. Vigderman, S. D. Evans, E. R. Zubarev, and N. A. Kotov, *Adv. Mater.* 2010, **22**, 2338-2342.
- 6 C. R. Carey, T. Lebel, D. Crisostomo, J. Giblin, M. Kuno and G. V. Hartland, *J. Phys. Chem. C*, 2010, **114**, 16029-16036.
- 7 A. E. Siegman, *Lasers*, University Science Books, 1986.
- 8 P. B. Johnson and R. W. Christy, *Phys. Rev. B* 1972, **6**, 4370-4379.